

# Influence of the Metal Oxide Substrate Structure on Vanadium Oxide Monomer Formation

Alexis M. Johnson · Brian R. Quezada ·

Laurence D. Marks · Peter C. Stair

Published online: 17 October 2013  
© Springer Science+Business Media New York 2013

**Abstract** Vanadium oxide ( $\text{VO}_x$ ) molecular species supported on high surface area oxide supports are active catalysts for oxidative transformations of organic molecules. Since the reactivity of  $\text{VO}_x$  species depends on their molecular structure, the understanding and control of factors that determine their structure would be useful in surface molecular catalyst design. Reactive adsorption of vanadyl triisopropoxide (VOTP) to form monomeric  $\text{VO}_x$  species on amorphous  $\text{Al}_2\text{O}_3$  and  $\text{SrTiO}_3$  (001) surfaces has been studied by X-ray photoelectron spectroscopy (XPS). Quantitative comparison of C(1s) and V(2p<sub>3/2</sub>) peak areas has been used to determine the number of isopropoxide ligands that are replaced by V–O surface bonds. On average, three V–O surface bonds are formed during adsorption on an amorphous  $\text{Al}_2\text{O}_3$  surface, as expected in the formation of a tridentate,  $\text{VO}_4$  structure, typically assigned to monomeric, surface  $\text{VO}_x$  species. On the  $\text{SrTiO}_3$  (001) surface, the number of V–O surface bonds depends on the oxygen density prior to reaction with VOTP. For

adsorption on the  $\text{SrTiO}_3$  surface cleaned and oxygen-annealed in ultrahigh vacuum, the number of V–O surface bonds is ca. 2. When the  $\text{SrTiO}_3$  surface has been Ar-ion sputtered prior to VOTP adsorption, the number of V–O bonds is ca. 1. This study demonstrates that the atomic structure of the support can strongly influence the molecular nature of surface  $\text{VO}_x$  species.

**Keywords** Vanadium oxide · Strontium titanate · XPS · Surface structure

## 1 Introduction

Supported vanadium oxide catalysts are industrially important for many catalytic reactions, including oxidative dehydrogenation of alkanes, desulfurization of fossil fuels and the production of sulfuric acid [1]. The structure of the  $\text{VO}_x$  species supported on a metal oxide has been extensively investigated in efforts to elucidate structure/catalytic reactivity relationships. IR, Raman, UV–Vis, EXAFS and NMR experiments have identified that several  $\text{VO}_x$  surface species exist: namely monomeric vanadyl units, polymeric chains and crystalline vanadia [1–4]. At low vanadia surface densities the surface species are expected to be mostly isolated vanadia monomers which consist of  $\text{VO}_4$  units [5]. Three identified monomer structures are shown in Scheme 1: (a) monodentate, (b) bidentate and (c) tridentate. These structures all have a single one-coordinate V=O, but differ by the number of V–O–M two-coordinate oxygen atoms that bridge between a vanadium atom and a metal cation of the support. Polymeric vanadia chains, 1d, form at higher surface concentrations and contain three oxygen atom coordinations: a single V=O, V–O–M

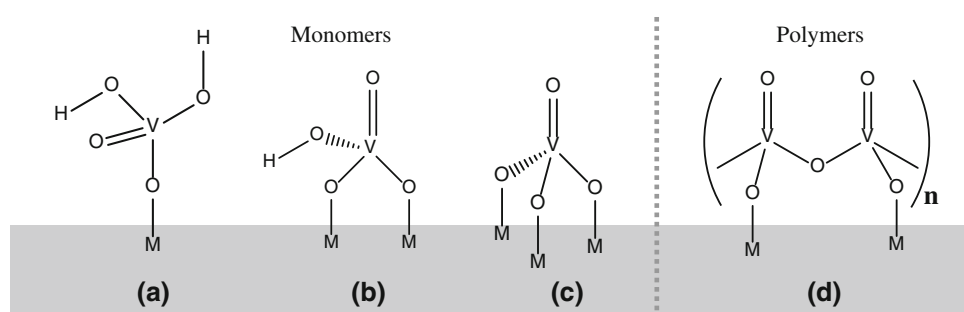
A. M. Johnson · P. C. Stair (✉)  
Department of Chemistry, Northwestern University, Evanston,  
IL 60208, USA  
e-mail: pstairst@northwestern.edu

B. R. Quezada  
McCormick School of Engineering, Northwestern University,  
Evanston, IL 60208, USA

L. D. Marks  
Department of Materials Science and Engineering, Northwestern  
University, Evanston, IL 60208, USA

P. C. Stair  
Chemical Sciences and Engineering Division, Argonne National  
Laboratory, Argonne, IL 60439, USA

**Scheme 1** Illustrations of vanadia monomers (**a–c**) and a polymeric chain (**d**). **a** Monodentate, **b** bidentate, and **c** tridentate vanadia monomer structures

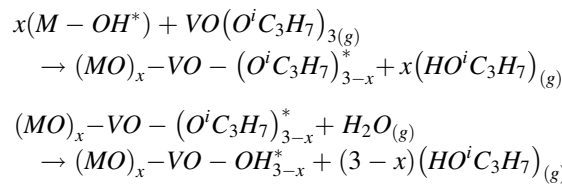


bridging oxygen atoms and V–O–V bridging oxygen atoms that connect one unit to another.

As the surface density increases it is less clear which species are present [6]. This problem is further complicated because the surface species are influenced by the composition and surface structure of the metal oxide substrate. While most researchers believe that the V–O–M bond can be catalytically active a debate still exists as to which lattice oxygen sites are active and about the number and types of each oxygen site as dictated by the type of  $\text{VO}_x$  species present on the surface [7, 8]. Further it has been shown that the different vanadia monomeric structures can exhibit substantially different reactivity [7]. In order to fully understand the mechanistic details of vanadia catalyzed reactions it is crucial to characterize the monomeric species that are present on a surface and the factors that influence the formation of specific species. For example, a subset of the species in a mixture may be largely responsible for the overall catalytic activity depending on the conditions of temperature and pressure and on the reaction under study. The development of methods to prepare species with the desired activity and/or selectivity would lead to improvements in catalyst performance.

There are several methods for synthesizing supported vanadia catalysts, namely grafting [9], wet impregnation [1] and recently atomic layer deposition (ALD) [10]. ALD is a promising technique for the synthesis of novel catalytic materials, where two sequential gas-surface reactions are cycled to grow metals, oxides and other materials in a layer-by-layer fashion [11, 12]. After one cycle, the initial surface functional groups are regenerated, providing new reaction sites for the following cycle. Since there are a finite number of surface reaction sites accessible, only a finite number of precursor molecules can react, leading to the self-limiting nature of ALD. The limited availability of reaction sites results in the ability to control growth of thin films at the atomic scale.

Previous experiments investigated the deposition of vanadyl triisopropoxide (VOTP) for the formation of vanadia thin films and supported vanadates [10, 13–16]. The reaction is believed to proceed by the mechanism:



where M is the support cation, X is the number of surface hydroxyl groups that undergo exchange with the VOTP ligands, and the asterisk denotes a surface species. The mechanism above implies that the number of isopropoxide ligands lost on the adsorbed vanadyl species after the surface reaction will be informative about the number of two-coordinate, oxygen bridge bonds, M–O–V or V–O–V, to the deposited V atoms. The number of bonds formed can shed light on which surface species was formed: a monodentate, bidentate, or tridentate  $\text{VO}_4$  unit [8].

In this study we utilize X-ray photoelectron spectroscopy (XPS) to explore the nature of supported  $\text{VO}_x$  species, deposited by atomic layer deposition, by correlating the number of ligands lost to properties of the surface, such as the structure and oxygen atom surface density.

## 2 Experimental Section

### 2.1 Instrumentation and Sample Mounting

All experiments were performed in an ultrahigh vacuum (UHV) apparatus with a base pressure in the range  $2\text{--}5 \times 10^{-10}$  Torr. The apparatus, which has been described previously [17], includes an Extrel quadrupole mass spectrometer (QMS), low energy electron diffraction (LEED), ion sputtering gun, heated dosing lines, high pressure cell and a dual-anode Thermo/VG Microtech X-ray photoelectron spectrometer with a hemispherical electron energy analyzer. A  $360^\circ$  rotating XYZ manipulator with a 1 meter Z-translator was used to position the sample for sputtering, gas dosing, and analytical measurements.

A  $\text{SrTiO}_3$  (001) single crystal (MTI) was mounted on a piece of nickel foil (Goodfellow) with silver loaded

electrode paste (Dupont 7095). Two 0.5 mm Ni:Cr (80:20) wires, spot-welded to the back of the foil, were used to suspend the sample between two thermally isolated copper leads on the bottom of the manipulator shaft. The sample was resistively heated and cooled with liquid nitrogen. The sample temperature was measured with a C-type thermocouple spot welded to the back of the Ni foil. The  $\text{SrTiO}_3$  (001) crystal was cleaned with argon ion sputtering using 2 keV ions at normal incidence followed by annealing in dry oxygen at a pressure of  $10^{-7}$  Torr for several hours at 863 K. XPS was used to verify that all of the contaminants had been removed. For experiments performed on a clean  $\text{SrTiO}_3$  (001) crystal, the crystal plane was verified by LEED.

In a separate reactor 25 cycles of trimethylaluminum and water were dosed forming a thin film of  $\text{Al}_2\text{O}_3$  on a  $\text{SiO}_2/\text{Si}$  substrate at 498 K. The calculated film thickness based on measured growth per cycle was 27.5 Å. Unlike the  $\text{SrTiO}_3$  crystal, the alumina sample was mounted on Ni foil with Ta foil clips to reduce the damage done to the alumina film from sample handling. Extended use of ion sputtering was prohibited due to the damage caused by sputtering. However, light Ar ion sputtering was able to remove most of the initial carbon contaminants.

## 2.2 Atomic Layer Deposition

$\text{VO}_x$  films were grown at substrate temperatures ranging from 373–473 K with alternating exposures of vanadyl tri-isopropoxide (VOTP, Sigma-Aldrich 99.98 %) and water. The VOTP and water vessels were kept at room temperature where the vapor pressures of the liquids are 0.045 and 33 Torr, respectively [18, 19]. Freeze–pump–thaw cycles were performed on both precursors until there was no evidence of air in the precursor, detected by QMS. Leak valves were used to introduce the 300 K gaseous precursors for directed dosing of the surface, during which the chamber pressure rose to  $1 \times 10^{-6}$  Torr. The saturation exposure time for VOTP and water was 3 and 10 min (180 and 600 Langmuir doses), respectively. After dosing was completed, the chamber was evacuated to a pressure of  $10^{-8}$  Torr before analysis. Oxygen satellite peaks overlapping the  $\text{V}(2\text{p}_{3/2})$  region were removed through subtraction of background spectra taken prior to precursor dosing. Due to sample charging and nonlinearity in the XPS spectrometer, the C(1s) peak from the alkoxide group in the ligand was referenced to a binding energy of 286.4 eV, the expected binding energy of a surface bound alkoxide [20]. The  $\text{V}(2\text{p}_{3/2})$  binding energies were referenced to the O(1s) binding energy of the respective substrate: 531.0 eV for  $\text{Al}_2\text{O}_3$  and 529.2 eV for  $\text{SrTiO}_3$  [21, 22].

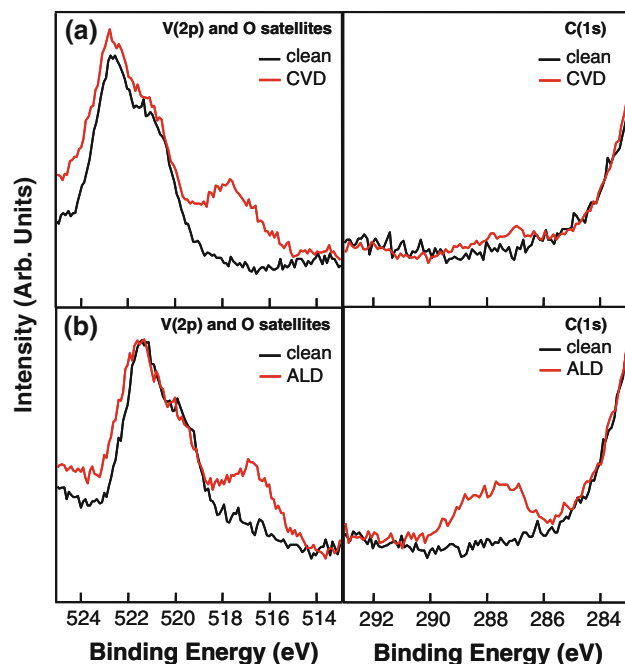


**Fig. 1** Comparison of the V(2p) and C(1s) spectra grown through **a** CVD and **b** ALD processes

## 3 Results

### 3.1 Self-Limiting Reactions

While atomic layer deposition has been performed in UHV chambers [23–25], the self-limiting nature of the reaction was verified for our experimental apparatus. Previous experiments have identified that the ALD temperature window for VOTP is 353–423 K [14]. In excess of 423 K the growth mode changes from self-limiting to chemical vapor deposition (CVD). During CVD the substrate temperature is greater than the decomposition temperature of the precursor resulting in flux dependent growth of the film. Figure 1 illustrates growth above and below the decomposition temperature of VOTP. The  $\text{V}(2\text{p}_{3/2})$ , O(1s) and C(1s) spectra before and after one VOTP dose are shown in the black and red lines, respectively. When the substrate temperature is 473 K the vanadium signal increases while the change in the carbon signal is almost negligible (Fig. 1a), indicating all three ligands reacted with the surface and decomposed into volatile products. As shown in Fig. 1b, when the surface temperature is below the decomposition temperature, both the  $\text{V}(2\text{p}_{3/2})$  and C(1s) signals increase upon exposure to the surface. This result suggests that a fraction of the ligands from the precursor have remained on the surface after deposition, as expected in an ALD process. While this result is not direct evidence of ALD, it does corroborate the previously identified ALD

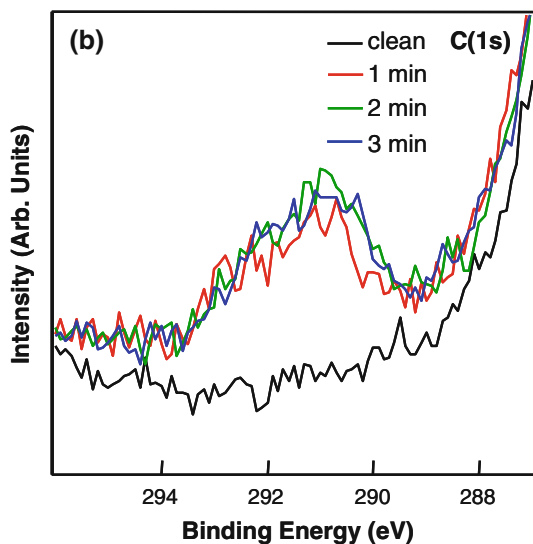
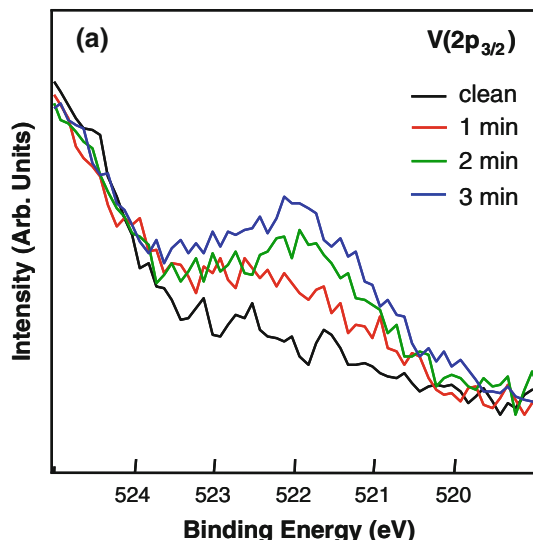


**Fig. 2** **a**  $V(2p)$  and **b**  $C(1s)$  signal as a function of increasing VOTP exposure time

temperature window and demonstrates the ability to distinguish between CVD and ALD by XPS measurements.

The self-limiting behavior of atomic layer deposition is verified with the exposure time dependence of VOTP deposition at a substrate temperature of 373 K, shown in Fig. 2. The black line is the initial V and C signals and the red, green and blue lines represent sequential 1 min doses of VOTP for a total of 1, 2 and 3 min of dosing onto the sample. In Fig. 2b the  $C(1s)$  signal reaches saturation near an exposure time of 2 min indicating that the surface is saturated and that additional carbon is not deposited during the third minute of exposure. In Fig. 2a, the  $V(2p_{3/2})$  signal continues to increase slightly between 2 and 3 min of dosing, indicative of so called “soft saturation” [26]. This increase is likely the result of the high background pressure of water inside the chamber, which regenerates additional

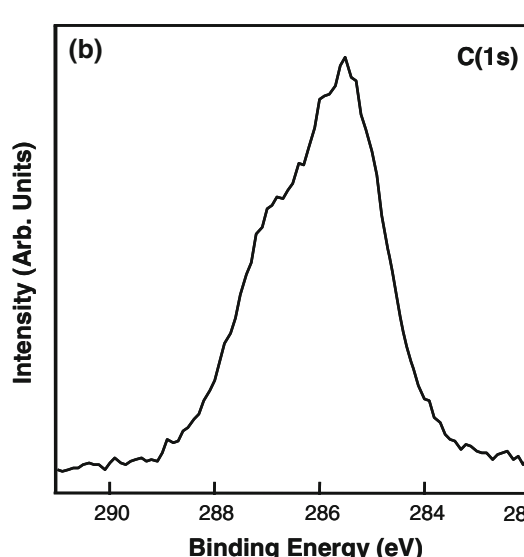
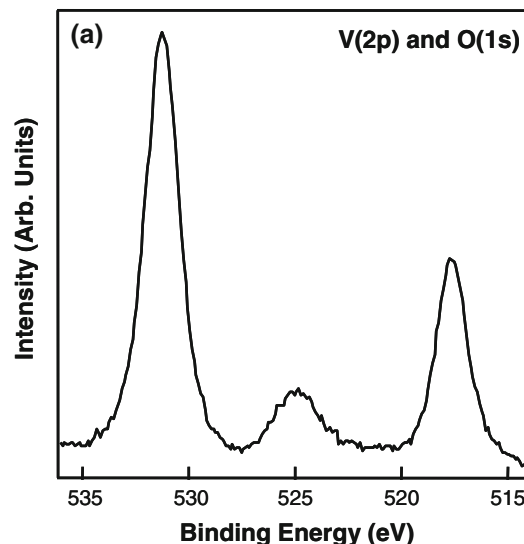


**Fig. 3** **a**  $V(2p)$  and **b**  $C(1s)$  spectra taken from condensed VOTP

surface hydroxyl groups between VOTP doses. The results from the temperature dependence and exposure time dependence experiments demonstrate that at a surface temperature of 373 K  $VO_x$  can be grown in the UHV apparatus in an ALD-like fashion.

### 3.2 Vanadyl Triisopropoxide Deposition

#### 3.2.1 Condensed Precursor Measurements

Ratios of the  $V(2p_{3/2})$  to  $C(1s)$  peak areas in the XPS spectra were used to investigate the  $VO_x$  deposition process. In the absence of adventitious carbon the  $C(1s)$  signal is a direct measure of the carbon in the isopropoxide ligands on the surface. The ratio of  $V(2p_{3/2})$  to  $C(1s)$  signals of an intact VOTP molecule was used to verify that the

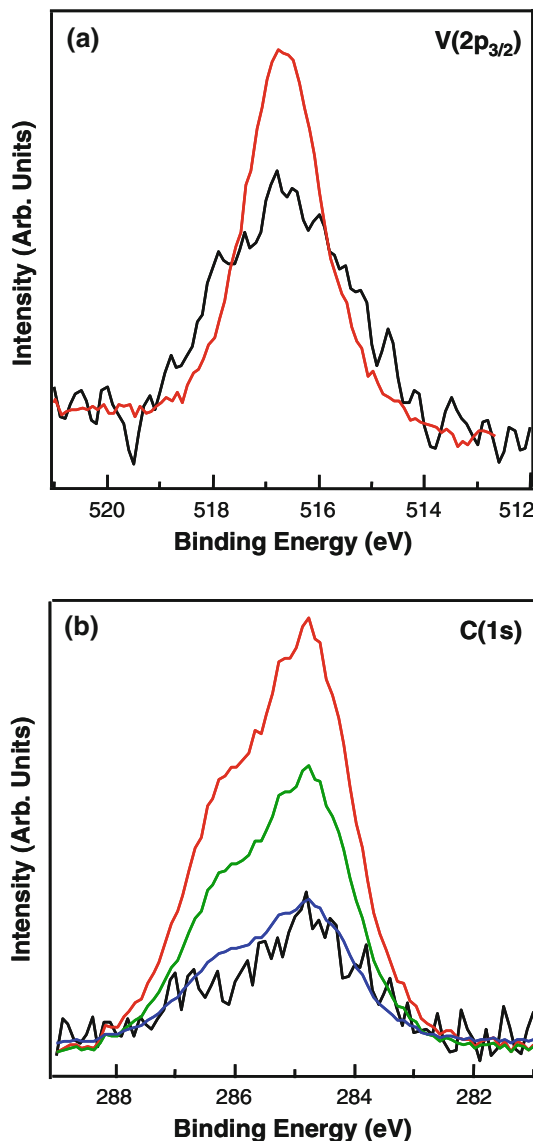


**Fig. 4** VOTP deposited onto ALD formed alumina. **a** V(2p<sub>3/2</sub>) spectra of the deposited vanadia (black) and scaled condensed precursor (red). **b** C(1s) spectra of the deposited vanadia (black) while the red, green and blue lines represent the intact VOTP molecule, 1 ligand lost and 2 ligands lost, respectively

precursor was not decomposing before reaching the surface and to provide a reference for the ratio of intensities expected when all three ligands remain on the molecule. VOTP condensed onto a liquid-nitrogen-cooled sample produced the V(2p<sub>3/2</sub>) and C(1s) spectra shown in Figs. 3a, b, respectively. The C(1s) signal is a combination of two peaks in a 2:1 area ratio. These peaks correspond to the two different carbon environments in an isopropoxide ligand. The V:C intensity ratio, corrected for elemental sensitivity, is 1:9.5 [27]. The measured ratio is slightly higher than expected for VO(C<sub>3</sub>H<sub>7</sub>O)<sub>3</sub>, due to condensation of contaminant isopropyl alcohol in the dosing gas resulting from

**Table 1** Summary Figs. 5, 6 and 7, including the vanadium surface density, average number of ligands lost, V(2p<sub>3/2</sub>) peak binding energy and full width half maximum for each substrate

Substrate	V added (V/nm <sup>2</sup> )	Avg. ligands lost	Peak BE (eV)	FWHM (eV)
Al <sub>2</sub> O <sub>3</sub>	2.8 ± 0.2	2.2 ± 0.2	516.7	3.3
SrTiO <sub>3</sub> (001)	1.8 ± 0.2	1.9 ± 0.2	516.0	2.5
SrTiO <sub>3</sub> (001) sputtered	1.9 ± 0.2	1.1 ± 0.2	516.0	2.7

VOTP decomposition or inaccuracy of the elemental sensitivity factors.

The spectrum of condensed VOTP is used as a guide for the deposition onto different substrates. The vanadium and carbon signals in Fig. 3 provide a calibration for the situation where none of the ligands react and desorb off the surface. A measured carbon signal, normalized to the vanadium signal, corresponding to 66 or 33 % that of condensed VOTP, indicates the loss of one or two ligands, respectively.

### 3.2.2 Vanadyl Triisopropoxide Deposition onto ALD-Formed Alumina

The results from VOTP deposition onto a film of Al<sub>2</sub>O<sub>3</sub> supported on a silicon wafer are shown in Fig. 4. The black lines represent the measured vanadium and carbon signals after deposition. In Fig. 4a, the red line corresponds to the V(2p<sub>3/2</sub>) spectrum of condensed VOTP, scaled to have a peak area equivalent to the deposition spectrum. The V(2p<sub>3/2</sub>) spectrum from VOTP deposition is broader than from the condensed layer due to inhomogeneity in the environments surrounding the deposited vanadium atoms compared to condensed molecular VOTP where vanadium has only one bonding environment with all three ligands still intact. The full width half maximum is 3.3 eV, which is slightly broader than previously observed V(2p<sub>3/2</sub>) spectra from deposited vanadia species [28, 29]. Peak broadening is observed for all V(2p<sub>3/2</sub>) spectra taken after deposition. The peak has a binding energy of 516.7 eV which is similar to the reported V<sup>5+</sup> binding energy of 516.9 eV [30]. The data from all of the VOTP deposition experiments is summarized in Table 1, including the deposited V surface concentration, average number of ligands lost, peak binding energy and the full width half maximum for each substrate.

The number of vanadium atoms per square nanometer can be calculated by a procedure used previously to calculate the surface coverage of adsorbed methyl radicals on Fe<sub>3</sub>O<sub>4</sub> (111) [31]. Based on the density of aluminum atoms in ALD deposited films (4 Al atoms/nm<sup>2</sup>), an effective sampling depth equivalent to the inelastic mean free path

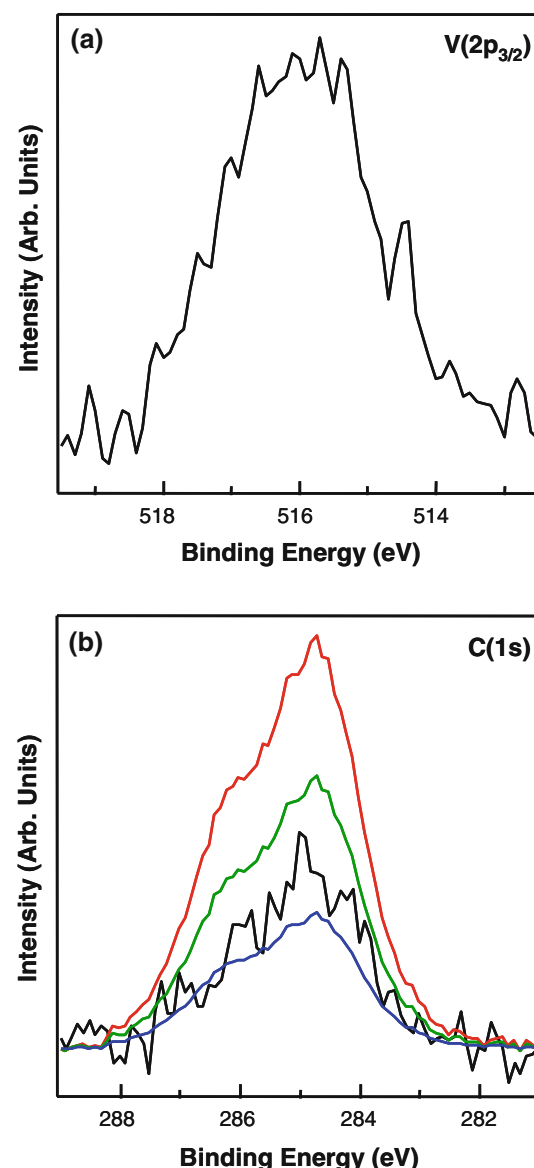
(20 Å in alumina using the Mg K $\alpha$  X-ray source), deposition of 1.1 Å of alumina/cycle and the V:Ti peak area ratio adjusted for elemental sensitivities, the calculated vanadium surface density on the alumina surface was approximately  $2.8 \pm 0.2$  V atoms/nm<sup>2</sup> [32, 33].

Figure 4b shows the C(1s) signals from condensed VOTP and after the deposition (black). The red line is the expected intensity of intact VOTP obtained by normalizing to the V(2p<sub>3/2</sub>) deposition spectrum. The green and blue lines are 66 and 33 % of the intensity expected for intact VOTP (red line), corresponding to the spectra predicted for a loss of 1 and 2 ligands, respectively. The peak shape of the C(1s) spectrum resulting from deposition is similar to the condensed VOTP spectrum, indicating that the signal after deposition is largely composed of carbon atoms in isopropoxide ligands. The deposition spectrum falls below the blue line, indicating that on average VOTP molecules will lose 2–3 ligands upon reaction with an ALD-formed alumina surface at 373 K. The ratio of the peak areas of the C(1s) deposition spectrum and the intact VOTP spectrum yields an average of  $2.2 \pm 0.2$  ligands lost per molecule. The XPS spectra only provide information about the average number of ligands lost over all deposited molecules which likely have a distribution of ligands lost. This result implies that there are several scenarios for the VOTP molecules to bond to an alumina surface leading to the loss of 1, 2 and even 3 ligands.

### 3.2.3 Vanadyl Triisopropoxide Deposition onto Strontium Titanate (001)

The results of a single dose of VOTP onto a clean SrTiO<sub>3</sub> (001) crystal at 393 K are shown in Fig. 5. In Fig. 5a the black line represents the measured vanadium signal after deposition. The full width half maximum is 2.5 eV with a binding energy of 516.0 eV. The broadening observed is closer to the widths found in the literature for deposited species, however the binding energy is lower than expected. The surface density of vanadium atoms per square nanometer can be calculated to be  $1.8 \pm 0.2$  V atoms/nm<sup>2</sup>, based on the density of Ti atoms on a (1 × 1) terminated SrTiO<sub>3</sub> unit cell (6.56 Ti/nm<sup>2</sup>), an effective sampling depth equivalent to the inelastic mean free path (22.5 Å for Ti(2p) in SrTiO<sub>3</sub> using the Mg K $\alpha$  X-ray source [32]), and a TiO<sub>2</sub> plane separation of 3.905 Å along the (001) direction and the V:Ti peak area ratio.

Figure 5b shows the C(1s) signals from condensed VOTP and after the deposition (black). The red line is the expected intensity of intact VOTP obtained by normalizing to the V(2p<sub>3/2</sub>) deposition spectrum. The green and blue lines are 66 and 33 % of the intensity expected for intact VOTP (red line), corresponding to the spectra predicted for a loss of 1 and 2 ligands, respectively. The peak shape of



**Fig. 5** VOTP deposited onto a clean SrTiO<sub>3</sub> (001) single crystal. **a** V(2p<sub>3/2</sub>) spectra of the deposited vanadia (black) and scaled condensed precursor (red). **b** C(1s) spectra of the deposited vanadia (black) while the red, green and blue lines represent the intact VOTP molecule, 1 ligand lost and 2 ligands lost, respectively

the C(1s) spectrum indicates that the signal after VOTP deposition is largely composed of carbon atoms in isopropoxide ligands. The deposition spectrum sits just above the blue line, indicating that 1–2 ligands are lost upon reaction with a clean SrTiO<sub>3</sub> surface at 373 K. The ratio of the peak areas of the C(1s) deposition spectrum and the intact VOTP spectrum yields an average of  $1.9 \pm 0.2$  ligands lost per molecule.

Vanadyl triisopropoxide was also deposited onto a clean SrTiO<sub>3</sub> (001) crystal, which had been sputtered with Ar ions but not annealed. It is well known that sputtering leads to a surface with structural defects and is often oxygen

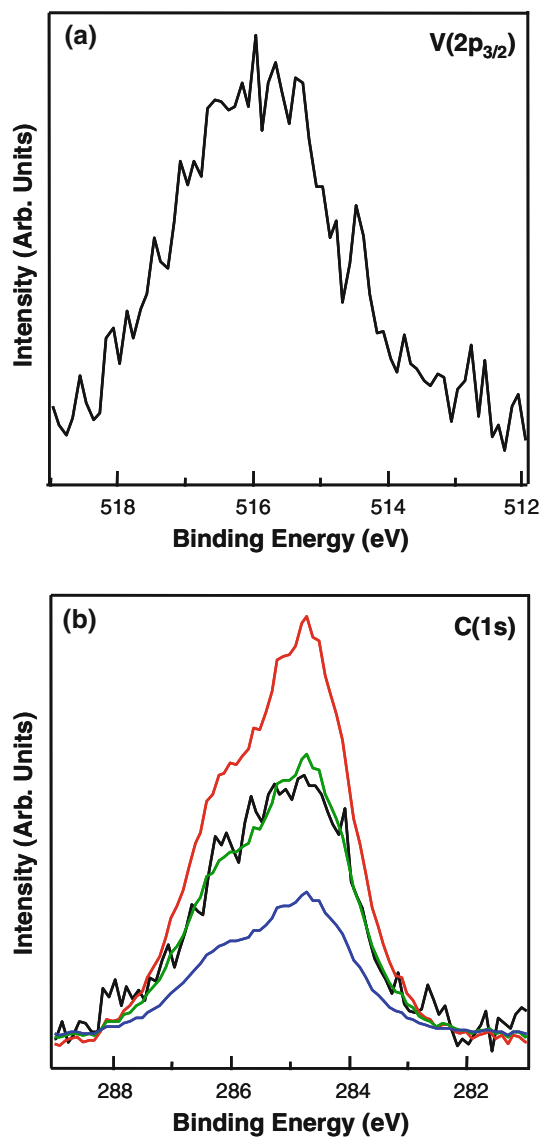


**Fig. 6** VOTP deposited onto an Ar ion sputtered  $\text{SrTiO}_3$  (001) single crystal. **a**  $\text{V}(2\text{p}_{3/2})$  spectra of the deposited vanadia (black) and scaled condensed precursor (red). **b**  $\text{C}(1\text{s})$  spectra of the deposited vanadia (black) while the red, green and blue lines represent the intact VOTP molecule, 1 ligand lost and 2 ligands lost, respectively

deficient. The results are shown in Fig. 6 where Fig. 6a, b show the  $\text{V}(2\text{p}_{3/2})$  spectra and  $\text{C}(1\text{s})$  spectra, respectively. The  $\text{V}(2\text{p}_{3/2})$  peak binding energy is 516.0 eV with a calculated vanadium surface density of  $1.9 \pm 0.2 \text{ V atoms/nm}^2$ . The normalized condensed VOTP  $\text{C}(1\text{s})$  reference signals (red, green and blue) are shown in Fig. 6b. The signal resulting from deposition (black) falls almost on top of the green line indicating that the deposited VOTP molecules average one ligand lost. The ratio of the peak areas of the  $\text{C}(1\text{s})$  deposition spectrum and the intact VOTP spectrum yields an average of  $1.1 \pm 0.2$  ligands lost per molecule. The  $\text{C}(1\text{s})$  spectra have a similar peak shape as in

Fig. 3b, 4b, and 5b, consistent with carbon atoms in isopropoxide ligands.

## 4 Discussion

### 4.1 Self-Limiting Behavior

Previous studies of thin film growth have indicated that ALD reactions typical of higher pressures will also occur in UHV environments [23–25]. The  $\text{V}(2\text{p}_{3/2})$  signal continually increased as a function of exposure time. This increase of signal is likely the result of residual water in the UHV chamber reacting with the surface and regenerating hydroxyl groups during the long measurement times. The lack of growth of the  $\text{C}(1\text{s})$  signal at long exposure times indicates that the reaction of VOTP with the surface of  $\text{SrTiO}_3$  is self-limiting. This behavior is evidence that our UHV dosing technique is also an ALD process and confirms that the information obtained from these experiments can provide direct insight into the reactions taking place at 10 Torr in typical ALD reactors.

The observed temperature window in this work agrees with literature values, where decomposition of VOTP occurs at temperatures in excess of 423 K [34]. Under CVD the ligands on the precursor molecules are converted to volatile products that desorb from the surface, and the film growth is dependent on the flux of the impinging precursor. When the surface is above the decomposition temperature of VOTP, CVD occurs and, in an adventitious carbon-free environment, a surface carbon signal will not be observed. Alternatively, below the decomposition temperature ALD occurs and the ligands remain on the surface leading to a visible carbon signal. The appearance of a  $\text{C}(1\text{s})$  signal or lack thereof is indicative of the deposition process taking place.

### 4.2 Comparison of the Substrate Surface Structures

The substrates used in these experiments included: ALD-formed  $\text{Al}_2\text{O}_3$ , clean  $\text{SrTiO}_3$  (001), and sputtered  $\text{SrTiO}_3$  (001). Under UHV conditions and following sputtering and annealing one might expect oxide surfaces to be completely dehydrated. However, there is evidence that surface OH groups are remarkably persistent on the  $\text{SrTiO}_3$  (100) surface following treatments similar to those used in the present study [35, 36]. Since the ALD-formed  $\text{Al}_2\text{O}_3$  was subjected to significantly milder treatment in UHV, we expect it to be an amorphous, hydrated thin film on the oxide covered silicon wafer. Quartz crystal microbalance studies of alumina ALD have obtained a reactive surface OH density for ALD alumina of  $6.2/\text{nm}^2$  [37]. Molecular dynamics simulations of amorphous alumina are in

agreement with this surface density and indicate that the OH-groups are primarily bonded to 1 or 2 aluminum atoms in approximately a 2:1 ratio [38].

$\text{SrTiO}_3$  in the (001) orientation has a bulk, cubic perovskite structure with alternating layers of  $\text{TiO}_2$  and  $\text{SrO}$ . Previous experiments have observed several surface reconstructions for the (001) plane including  $(2 \times 1)$ ,  $(2 \times 2)$ ,  $c(4 \times 2)$ ,  $c(4 \times 4)$ ,  $c(6 \times 2)$ ,  $(6 \times 2)$ ,  $(\sqrt{5} \times \sqrt{5})$ -R26.6° and  $(\sqrt{13} \times \sqrt{13})$ -R33.7° (RT13) [35, 36, 39–46]. In the current work the sample was sputtered and annealed at 850 K in  $10^{-7}$  Torr of oxygen. Identifying the surface reconstruction of the crystal was attempted, however only a  $(1 \times 1)$  pattern was observed which is consistent with the relatively low annealing temperature. Based upon prior work for the RT13 structure [43] this surface is likely to be a disordered glass consisting of (a)  $\text{TiO}_5[]$  units where “[]” is a vacancy in the octahedral co-ordination of the Ti, with perhaps some tetrahedrally coordinated  $\text{TiO}_4$  units at defects (similar to what has been observed on the (110) surface, e.g. [47]), (b) domains of  $\text{SrO}$  termination, and (c) surface hydroxyl groups. Based on the sample preparation it is likely that  $\text{Ti}^{3+}$  ions are also present following sputtering [48]. However, due to the large bulk  $\text{Ti}^{4+}$  signal reduced Ti atoms were not directly observed in the XPS spectra. Assuming all O atoms remain from the bulk  $(1 \times 1)$  structure, the surface oxygen density is approximately 13 O atoms/ $\text{nm}^2$ .

The third surface was a  $\text{SrTiO}_3$  (001) surface that was prepared in the same manner as the first, except that as a final step prior to deposition the crystal was sputtered once more with Ar ions without further annealing, leaving the surface with structural defects and probably enriched in  $\text{TiO}_2$ . Since sputtering has been shown to alter the local geometries of a surface by preferentially removing oxygen atoms from the lattice resulting in reduced metal atoms, the comparison of this surface with the previous one provides information on the role of surface oxygen density in determining the species formed by VOTP adsorption [49].

#### 4.3 Formation of Vanadia Monomers on Metal Oxide Surfaces

##### 4.3.1 Vanadia Monomer Structures

Based on the low vanadia surface densities, summarized in Table 1, it is likely that the VOTP deposition onto alumina and  $\text{SrTiO}_3$  (001) surfaces results in the formation of  $\text{VO}_x$  monomers with the possibility of some polymers present on the alumina [50]. Previous experiments of supported vanadium oxide included substrates of  $\text{NbO}_2$ ,  $\text{TiO}_2$ ,  $\text{CeO}_2$ ,  $\text{Ta}_2\text{O}_5$ ,  $\text{ZrO}_2$ , two  $\text{SiO}_2$  substrates, Aerosil 300 and SBA-15, and  $\alpha$ ,  $\kappa$  and  $\theta$ - $\text{Al}_2\text{O}_3$  [8, 51–58]. Investigations include studies of oligomer or polymer formation, dispersion and

comparing substrate effects. Few studies have characterized the exact vanadia monomer species present on the surface. UV Raman experiments coupled with DFT calculations on  $\theta$ -alumina have suggested several structures for monomeric vanadia: “monodentate”, “bidentate” and “tridentate” as shown previously in Scheme 1 [8]. All species contain a doubly coordinated oxygen atom on the vanadium atom. The “monodentate” structure has one bond to the surface and a hydrogen bond from the 2-coordinated oxygen to a neighboring surface hydroxyl group. The “bidentate” structure has two bonds to the surface. The “tridentate” structure has three bonds to the surface. There is also a fourth identified structure, “molecular” which also has two surface bonds. The difference between the “molecular” species and the “bidentate” species is that the “molecular” structure is bonded to the surface via bridging OH-groups rather than bridging O-atoms. Raman and UV–Vis spectroscopy have suggested that tridentate and bidentate monomer structures exist on silica [59]. X-ray diffraction and XPS experiments combined with Raman spectroscopy found that if a silica substrate was pretreated at 473 K bidentate monomers formed, whereas if the substrate was pretreated at 873 K the monodentate monomer formed. These studies have identified that a number of factors influence the formation of specific monomer structures, including the geometry and chemical composition of the surface and the ligand on the precursor [8, 60].

##### 4.3.2 Determination of Possible $\text{VO}_x$ Structures Through XPS

Due to the dependence of the molecular structure on the properties of the substrate it is challenging to predict which of the  $\text{VO}_x$  species will be present on a given surface. In this study the number of ligands lost upon deposition provides an insight into the possible vanadia species formed and the role of the metal oxide support structure. An average loss of 2–3 ligands from VOTP on amorphous alumina suggests that a distribution of vanadia monomers formed upon deposition where there was some combination of 1, 2 and all 3 ligands lost. There are a number of possible distributions that result in an average that is between 2 and 3. However, in all scenarios the majority of the monomers must be tridentate in order to have a distribution mean greater than 2. While it is possible that the high vanadium surface density of 2.8 V/ $\text{nm}^2$  indicates some polymer formation, previous work provides strong evidence that this is not the case [10].

For deposition onto the clean  $\text{SrTiO}_3$  crystal and the sputtered  $\text{SrTiO}_3$  surface the vanadium surface densities of 1.8 and 1.9 V atoms/ $\text{nm}^2$  suggest that both surfaces contain isolated vanadia monomers. The average loss of 1–2

ligands upon deposition onto the clean  $\text{SrTiO}_3$  crystal is consistent with several possible monomer species making it difficult to narrow down their structures based on this information alone. However, for the sputtered  $\text{SrTiO}_3$  crystal an average of only 1 ligand was lost during VOTP deposition, indicating that the majority of the monomers are monodentate. The presence of adsorbed VOTP with 2 or 3 ligands lost would require a significant, compensating population of intact, molecular adsorbed VOTP. We discount this possibility under our experimental conditions of ultrahigh vacuum and 373 K sample temperature.

A natural correlation to draw would be between the number of ligands lost and the density of reactive sites on the support surface. The crystal structure of vanadyl trimethoxide has a O–V–O separation of approximately 2.6–2.9 Å between the oxygen atoms [61]. From this data, the corresponding O–O distance for vanadyl triethoxide was estimated to be 2.6 Å [61, 62]. It is expected that VOTP would have a similar O–V–O separation, suggesting that for multiple ligands to react the surface oxygen atoms have to be approximately 2.6 Å apart. According to conventional ALD mechanisms the reactive sites are likely to be surface hydroxyl groups. The ALD formed alumina surface had the highest degree of hydration in part because the sample was exposed to water during the final step in the ALD synthesis and then to air before insertion into vacuum without annealing above 373 K. It is likely that the alumina film is hydroxyl terminated with a reactive OH density of  $\sim 6/\text{nm}^2$  added per cycle, based on mass gain per  $\text{cm}^2$  during ALD alumina growth [37]. 6 OH groups/ $\text{nm}^2$  is likely a minimum value because each ALD cycle does not fully cover the surface and oxygen atoms and hydroxyl groups from previous cycles could remain accessible for reaction.

The hydroxyl densities for the  $\text{SrTiO}_3$  surfaces were not quantified, but the sample preparation employed is expected to have produced dehydrated surfaces with a small amount of adsorbed water. Not only was the direct water exposure lower and the annealing temperature higher for the  $\text{SrTiO}_3$  substrates, but the Al–O bond is more ionic compared to the Ti–O bond and therefore an alumina surface will bond water more strongly than a  $\text{TiO}_2$ -terminated  $\text{SrTiO}_3$  surface. All of these factors indicate that both  $\text{SrTiO}_3$  surfaces had a lower density of hydroxyl groups than the  $\text{Al}_2\text{O}_3$  surface. It is expected that sputtered  $\text{SrTiO}_3$  has the lowest OH density due to the preferential removal of oxygen atoms, and hence hydroxyl groups by sputtering. The comparatively smaller density of surface OH groups on a sputtered surface would create fewer opportunities for losing multiple ligands per adsorbed VOTP molecule. Based on the available information, the order of the supports with increasing hydroxyl density is sputtered  $\text{SrTiO}_3$ , clean  $\text{SrTiO}_3$  and  $\text{Al}_2\text{O}_3$ . This order also correlates with the increase in the number of ligands removed from VOTP

upon reaction with each surface. This result suggests that the higher the reactive site density the higher the average number of ligands removed per VOTP molecule.

The surface oxygen density correlates with the number of ligands lost and more importantly the type of monomeric species can form on a surface. However, oxygen densities are an average across the entire surface and therefore better used to observe general trends rather than provide information about individual site specific monomer formation. Alternatively, the structure of the substrate may be more informative due to the direct influence it has on individual reaction sites and the O–O distances. While it is difficult to extensively discuss the alumina case because of its amorphous nature, it is likely that as the hydroxyl group density increases the OH groups will pack in a hexagonal close packed configuration similar to the packing of  $\text{Al}_2\text{O}_3$  (0001) as shown in Fig. 7. Figure 7 depicts the packing of a hydroxyl terminated crystalline  $\text{Al}_2\text{O}_3$  (0001) where the O anions are in light blue, Al cations are in red and the H atoms are purple. Oxygen atoms labeled A, B and C are three potential sites for the formation of a tridentate species. The packing results in an average distance of 2.5 Å between A, B and C, which is similar to the O–V–O separation, 2.6 Å, in vanadyl triethoxide. This implies that the reactive sites are close enough for the tridentate structure to form which is consistent with our observations. Due to the temperature of annealing during sample preparation the termination of the  $\text{SrTiO}_3$  crystal is unknown and likely glassy. Though under these conditions there are likely sections of RT13 reconstructions, as depicted in Fig. 8 where the O anions are in red, Ti cations are dark blue and the Sr cations are orange [43]. Similar to Fig. 7, there are three O atoms labeled A, B and C which are potential reactive sites for the formation of tridentate monomers. The lengths between A–B and A–C are close to the expected distance between O atoms in vandy triethoxide suggesting that VOTP may form bidentate structures between these two reactive sites. However, a third bond to the surface is less likely to form because of the increased distance, 3.8 Å, between atoms B and C. This also applies to the formation of a tridentate structure between oxygen atoms A, C and D because D resides in the  $\text{TiO}_2$  layer below A and C. While this is just one of the many surface terminations for  $\text{SrTiO}_3$ , the remaining known reconstructions on the (001) surface do not have three oxygen atoms in close enough proximity for the loss of three ligands [35, 36, 39–46]. Given the restraints from the surface structure, most monomeric species are expected to be either molecular, bi- or monodentate. Even though the surface was not clearly defined during these experiments there are strong correlations between the surface structure of the support and the number of ligands lost and more importantly the monomer species likely formed on the surface.

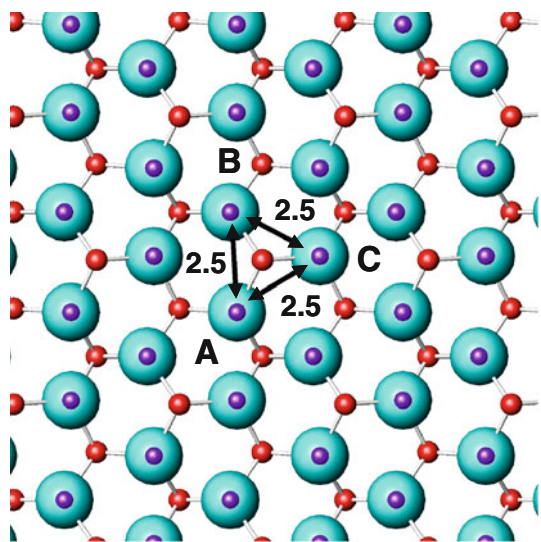


**Fig. 7** Hydroxyl terminated crystalline  $\text{Al}_2\text{O}_3$  (0001) surface. Oxygen atoms are blue, aluminum atoms are red and hydrogen atoms are purple. Oxygen atoms labeled A, B and C are potential reactive sites and are 2.5 Å apart

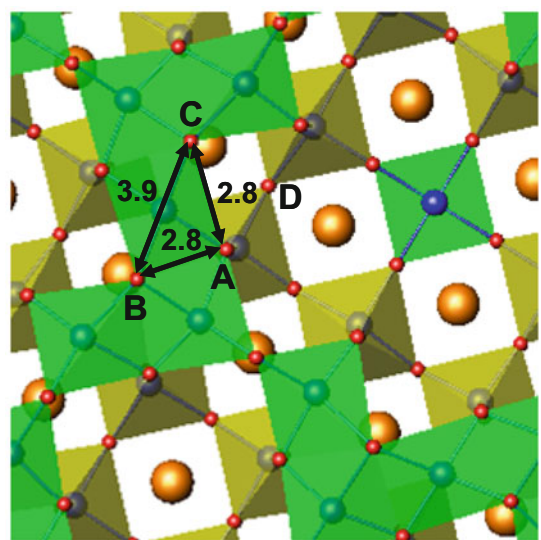


**Fig. 8** ( $\sqrt{13} \times \sqrt{13}$ )-R33.7° reconstruction of a  $\text{SrTiO}_3$  (001) surface [43]. Oxygen atoms are red, titanium atoms are blue and strontium atoms are orange. Oxygen atoms labeled A, B and C are potential reactive sites, distances between atoms are 2.8, 2.8 and 3.9 Å

#### 4.4 Vanadia Monomer Structure Influences on Reactivity

It is well documented that the reactivity of vanadia monomers is influenced by the composition of the metal oxide support. Wachs et al. [56] observed that the activity for methanol oxidation changed by several orders of magnitude depending on the support through the series:

$\text{SiO}_2 < \text{Al}_2\text{O}_3 < \text{Ta}_2\text{O}_5 < \text{Nb}_2\text{O}_5 < \text{TiO}_2 < \text{ZrO}_2 < \text{CeO}_2$ . In another study, they observed that propylene oxidation varied by a factor of  $\sim 20$  with the identity of the support [63]. In these two studies they concluded that the activity correlated with the electronegativity of the support cation. While the differences between polymeric and monomeric vanadia was considered, the possibility of different structural forms for the monomeric  $\text{VO}_x$  species was not discussed. However, Kim et al. [7] performed a spectroscopic study to delineate how the reactivity of vanadia monomers with hydrogen depends on the monomer structure. Experimentally, the bidentate structure reduced with  $\text{H}_2$  at a temperature nearly 100–200 K below the reaction temperature for the tridentate monomer. Computationally, the free energy barrier for the activation of  $\text{H}_2$  by the bidentate vanadia species is 17 kcal/mol lower than for the same reaction path by the tridentate species [7]. The same computations also demonstrate that  $\text{H}_2$  activation follows a radical abstraction mechanism very similar to the dominant mechanism for CH activation of alkanes [64, 65]. These observations indicate that the structure of vanadia monomers would be expected to have a large influence on the kinetics of the rate controlling step in  $\text{H}_2$  and CH activation. Supports with widely spaced oxygen atoms that make the trident vanadia structure unfavorable would be expected to stabilize the more reactive bidentate vanadia monomers and provide more active catalysts. The influence of oxide support geometry on the nature of vanadia monomer species have not yet been explored in detail and remains an unresolved issue in catalytic structure–function relationships.

## 5 Conclusions

It is challenging to directly identify specific vanadia monomer species on a metal oxide surface with XPS techniques alone. However, the average number of ligands lost from VOTP upon reaction with the oxide support along with the peak shape of the  $\text{V}(2\text{p}_{3/2})$  spectra can provide an insight into monomer formation. The majority of the vanadia monomers are tridentate on the surface of alumina, while for clean  $\text{SrTiO}_3$  the species could include a combination of tridentate, bidentate, monodentate and molecular monomer structures. Due to the lack of reactive sites on the sputtered  $\text{SrTiO}_3$  surface, the spectra indicate that only monodentate vanadia monomers are present. While there appears to be a correlation between the monomer species formed and the oxygen density of the metal oxide support, it is important to consider the structure of the surface because it dictates the distances between reactive oxygen atoms and therefore influences monomer formation. As previously shown, different monomer structures can result in different catalytic activity. This remains an

aspect of the catalytic structure–function relationship that is largely unknown.

**Acknowledgments** This material is based upon work supported by the National Science Foundation under Grant No. CHE-1058835. Brian Quezada acknowledges support from Chemical Sciences, Geosciences and Biosciences Division, Office of Basic Energy Sciences, Office of Science, US Department of Energy (Award DE-FG02-03-ER15457).

## References

1. Weckhuysen BM, Keller DE (2003) *Catal Today* 78:25
2. Ballarini N, Cavani F, Cericola A, Cortelli C, Ferrari M, Trifiro F, Capannelli G, Comite A, Catani R, Cornaro U (2004) *Catal Today* 91:2–99
3. Haber J, Kozlowska A, Kozlowski R (1986) *J Catal* 102:52
4. Khodakov A, Olthof B, Bell AT, Iglesia E (1999) *J Catal* 181:205
5. Wu Z, Kim H-S, Stair PC, Rugumini S, Jackson SD (2005) *J Phys Chem* 109:2793
6. Wu Z, Stair PC, Rugumini S, Jackson SD (2007) *J Phys Chem C* 111:16460
7. Kim H, Ferguson GA, Cheng L, Zygmunt SA, Stair PC, Curtiss LA (2012) *J Phys Chem C* 116:2927
8. Kim HS, Zygmunt SA, Stair PC, Zapol P, Curtiss LA (2009) *J Phys Chem C* 113:8836
9. Rice GL, Scott SL (1997) *Langmuir* 13:1545
10. Feng H, Elam JW, Libera JA, Pellin MJ, Stair PC (2010) *J Catal* 269:421
11. George SM (2010) *Chem Rev* 110:111
12. Stair PC (2012) *Top Catal* 55:93
13. Keranen J, Guimon C, Iiskola E, Auroux A, Niinisto L (2003) *J Phys Chem B* 107:10773
14. Badot JC, Ribes S, Yousfi EB, Vivier V, Pereira-Ramos JP, Baffier N, Lincot D (2000) *Electrochim Solid State Lett* 3:485
15. Badot JC, Mantoux A, Baffier N, Dubrunfaut O, Lincot D (2004) *J Mater Chem* 14:3411
16. Musschoot J, Deduytsche D, Poelman H, Haemers J, Van Meirhaeghe RL, Van den Berghe S, Detavernier C (2009) *J Electrochem Soc* 156:P122
17. Parker BR, Jenkins JF, Stair PC (1997) *Surf Sci* 372:185
18. Kanai H, Yoshikawa T, Sone T, Nishimura Y (2002) *React Kinet Catal Lett* 75:213
19. Wagner W, Pruss A (2002) *J Phys Chem Ref Data* 31:387
20. Schulz KH, Cox DF (1993) *J Phys Chem* 97:647
21. Pilleux ME, Grahmann CR, Fuenzalida VM (1994) *J Am Ceram Soc* 77:1601
22. Moulder JF, Sticke WF, Sobol PE, Bomben KD (1992) *Handbook of X-ray photoelectron spectroscopy*. Perkin-Elmer, Eden Praire
23. Schmidt D, Strehle S, Albert M, Hentsch W, Bartha JW (2008) *Microelectron Eng* 85:527
24. Lee SY, Jeon C, Kim SH, Kim Y, Jung W, An KS, Park CY (2012) *Jpn J Appl Phys* 51:100201
25. Ma Q, Guo HS, Gordon RG, Zaera F (2010) *Chem Mat* 22:352
26. Matero R, Rahtu A, Ritala M, Leskela M, Sajavaara T (2000) *Thin Solid Films* 368:1
27. Briggs DS, Seah MP (1990) *Practical surface analysis: Auger and X-ray photoelectron spectroscopy*, vol 1, 2nd edn. Wiley, Chichester
28. Hess C, Tzolova-Mueller G, Herbert R (2007) *J Phys Chem C* 111:9471
29. Hess C, Schloegl R (2006) *Chem Phys Lett* 432:139
30. Sawatzky GA, Post D (1979) *Phys Rev B Condens Matter* 20:1546
31. Liu L, Quezada BR, Stair PC (2010) *J Phys Chem C* 114:17105
32. Powell CJ, Jablonski A (2002) *J Surf Anal* 9:322
33. George SM (2010) *Chem Rev* 110:111
34. Badot JC, Ribes S, Yousfi EB, Vivier V, Pereira-Ramos JP, Baffier N, Lincot D (2000) *Electrochim Solid-State Lett* 3:485
35. Becerra-Toledo AE, Enterkin JA, Kienzle DM, Marks LD (2012) *Surf Sci* 606:791
36. Becerra-Toledo AE, Castell MR, Marks LD (2012) *Surf Sci* 606:762
37. Lu J, Stair PC (2010) *Langmuir* 26:16486
38. Adiga SP, Zapol P, Curtiss LA (2007) *J Phys Chem C* 111:7422
39. Erdman N, Poepelmeier KR, Asta M, Warschkow O, Ellis DE, Marks LD (2002) *Nature* 419:55
40. Erdman N, Warschkow O, Asta M, Poepelmeier KR, Ellis DE, Marks LD (2003) *J Am Chem Soc* 125:10050
41. Warschkow O, Asta M, Erdman N, Poepelmeier KR, Ellis DE, Marks LD (2004) *Surf Sci* 573:446
42. Lanier CH, van de Walle A, Erdman N, Landree E, Warschkow O, Kazimirov A, Poepelmeier KR, Zegenhagen J, Asta M, Marks LD (2007) *Phys Rev B* 76:04542
43. Kienzle DM, Becerra-Toledo AE, Marks LD (2011) *Phys Rev Lett* 106:176102
44. Lin YY, Becerra-Toledo AE, Silly F, Poepelmeier KR, Castell MR, Marks LD (2011) *Surf Sci* 605:L51
45. Becerra-Toledo AE, Marshall MSJ, Castell MR, Marks LD (2012) *J Chem Phys* 136:214701
46. Kienzle DM, Marks LD (2012) *CrystEngComm* 14:7833
47. Enterkin JA, Subramanian AK, Russell BC, Castell MR, Poepelmeier KR, Marks LD (2010) *Nat Mater* 9:245
48. Marshall MSJ, Becerra-Toledo AE, Payne DJ, Eggleston RG, Marks LD, Castell MR (2012) *Phys Rev B* 86:125416
49. Mayer JT, Diebold U, Maday TE, Garfunkel E, Electron Spectrosc J (1995) *Relat Phenom* 73:1
50. Wachs IE, Weckhuysen BM (1997) *Appl Catal A* 157:67
51. Du G, Lim S, Pinault M, Wang C, Fang F, Pfefferle L, Haller GL (2008) *J Catal* 253:74
52. Chlostka R, Tzolova-Muller G, Schlogl R, Hess C (2011) *Catal Sci Technol* 1:1175
53. Todorova TK, Ganduglia-Pirovano MV, Sauer J (2007) *J Phys Chem C* 111:5141
54. Wang QG, Madix RJ (2001) *Surf Sci* 474:L213
55. Ferreira ML, Volpe M (2000) *J Mol Catal A-Chem* 164:281
56. Wachs IE, Chen Y, Jehng JM, Briand LE, Tanaka T (2003) *Catal Today* 78:13
57. Baron M, Abbott H, Bondarchuk O, Stacchiola D, Uhl A, Shaiikhutdinov S, Freund HJ, Popa C, Ganduglia-Pirovano MV (2009) *J Sauer. Angew Chem-Int Ed* 48:8006
58. Penschke C, Paier J, Sauer J (2013) *J Phys Chem C* 117:5274
59. Wu Z, Dai S, Overbury SH (2010) *J Phys Chem C* 114:412
60. Wegener SL, Kim H, Marks TJ, Stair PC (2011) *J Phys Chem Lett* 2:170
61. Caughlan CN, Smith HM, Watenpau K (1966) *Inorg Chem* 5:2131
62. Inumaru K, Okuhara T, Misra M (1991) *J Phys Chem* 95:4826
63. Tian HJ, Ross EI, Wachs IE (2006) *J Phys Chem B* 110:9593
64. Rozanska X, Fortrie R, Sauer J (2007) *J Phys Chem C* 111:6041
65. Fu G, Xu X, Lu X, Wan H (2005) *J Phys Chem B* 109:6416